Supporting Information

Engineering deficient-coordinated Single-atom Indium Electrocatalyst for Fast Redox Conversion in Practical 500 Wh/kg-level Pouch Lithium-sulfur Batteries

Yang Guo, ‡ Zhaoqing Jin, ‡ Jianhao Lu, Lei Wei, Weikun Wang, * Yaqin Huang, * Anbang Wang *

[a] Research Institute of Chemical Defense, Beijing 100191, China

[b] Beijing Key Laboratory of Electrochemical Process and Technology for Materials, Key Laboratory of Biomedical Materials of Natural Macromolecules, Ministry of Education, Beijing University of Chemical Technology, Beijing 100029, China

‡These authors contributed equally to this work.

*Corresponding Author: Weikun Wang, Yaqin Huang, Anbang Wang

E-mail address: Wangweikun2022@163.com, huangyq@mail.buct.edu.cn, wab_wang2000@126.com

Experimental Section

Materials Characterization. The morphologies of the composites were observed by aberration-corrected scanning transmission electron microscopy (STEM, JEM-ARM200F) and Operando In K-edge XAS (beamline 01C1 at the National Synchrotron Radiation Research Center in Japan). X-ray diffraction (XRD) spectrum was collected on Bruker D2 Phaser diffractometer with Cu Kα radiation. In content was determined by Inductively coupled plasma optical emission spectroscopy (ICP-OES, 7300DV). The MFD-500AV-02 system was used to perform Mössbauer spectroscopy and a PerkinElmer Lambda 950 spectrometer for UV-vis measurements. VG Scienta R4000 analyzer and monochromatic He Ilight source (21.2 eV) were used to measure the Valance band (VB). secondary electron cutoff (SEC) was observed with a sample bias of -5V. The work function (ϕ) was determined by the difference between the photon energy and the secondary cutoff edge's binding energy.

Preparation of SAIn-N4@CNT. Following a similar procedure with SAIn-N3@CNT, SAIn-N4@CNT was created utilizing N-doped CNT in place of pure CNT. In more detail, N-doped CNT was produced by first heating CNT for two hours under NH_3 gas flow at a rate of 5 °C min^{-1} to 600 °C. Once the mass ratio of InPc to CNT reached 5:5 (w/w), the InPc solution with a concentration of 6 mg ml^{-1} was dropwise added to the CNT dispersion. Then, the centrifuged and dried composites were annealed for three hours at 680 °C in an environment of Ar gas flow to produce SAIn-N4@CN.

Assembly of Li-S coin cells. Li−S coin cells were assembled using the SAIn@CNT(or bare CNT) separators. The sulfur cathodes were prepared as described in our previous

papers[1]. Specifically, 89.6% S loading composite material, AB, and LA133 (the mass ratio is 72:20:8) were mixed in deionized water/isopropanol (volume ratio 4:1) to prepare the cathode slurries. The slurries were coated on Al foils and vacuum-dried at 60 ℃ for 12 h. The areal sulfur loading of the cathode is 1.5 mg cm^{-2}. Coin cells were assembled in CR2025 cases using 12 mm diameter cathodes, 19 mm diameter Li foils as anodes, and 19 mm diameter separators. The electrolyte was 1 M LiTFSI dissolved in DME/DOL (v/v,1:1) containing 2 wt % $LiNO_3$. The electrolyte/sulfur (E/S) ratio is controlled to 2 μl mg_s^{-1}.

Synthesis of Li_2S_6 electrolyte. The Li_2S and sublimed sulfur were weighed in the mass ratios of 1:5 and added to a traditional electrolyte (1 M LiTFSI in 1,3-dioxolane/dimethyl ether (1:1 v/v) mixture with 2.0 wt% $LiNO_3$), followed by vigorous magnetic stirring at 70 °C overnight thus yielding a brownish Li_2S_6 electrolyte (1 M).

Electrochemical evaluation. All samples are tested with a LAND CT2001A battery testing system in the fixed potential range of 1.8-2.6 V at 25 ℃. Electrochemical impedance spectroscopy (EIS) and Cyclic Voltammetry (CV) were carried out on an electrochemical workstation (VersaSTAT3). The details of nucleation and dissolution tests and adsorption tests are shown in Supporting Information section.

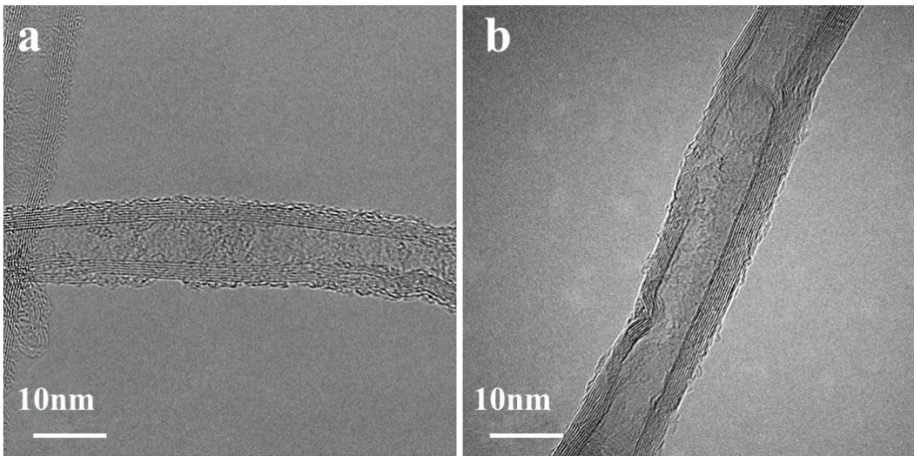

Figure S1. TEM images a) SAIn@CNT and b) CNT.

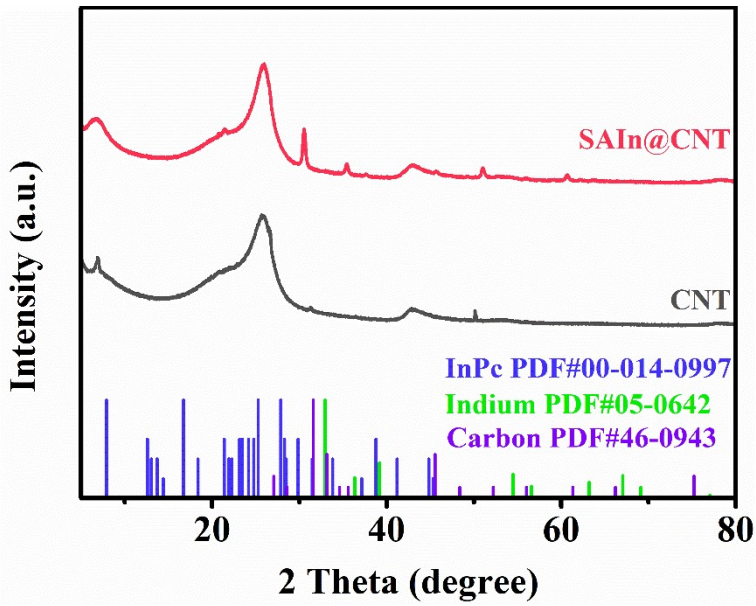

Figure S2. XRD patterns of SAIn@CNT and CNT.

By comparising the patterns of SAIn@CNT, CNT and the standard PDF card of In metal, InPc and carbon, we draw a conclusion that the peaks in the 2θ of 6.76°, 25.96°, 43°, 51.06° was attributed to CNT and the peaks in 30.54 may be attributed to carbon species (PDF#46-0943) produced by pyrolysis.

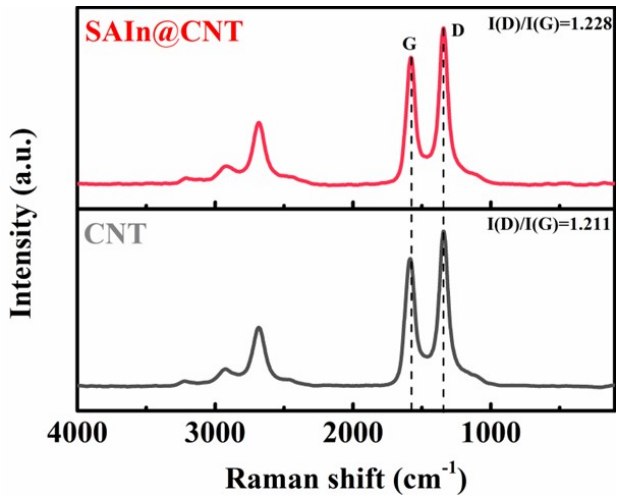

Figure S3. Raman curves of SAIn@CNT and CNT.

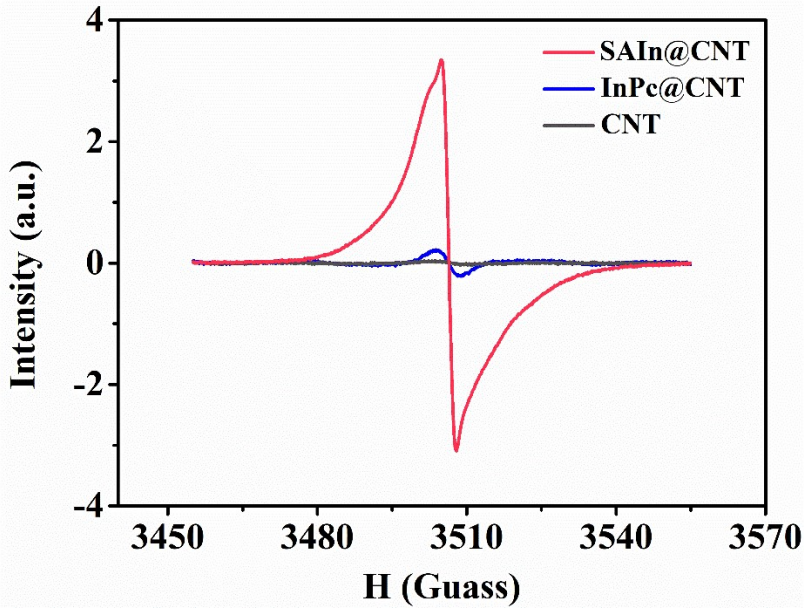

Figure S4. EPR spectra of SAIn@CNT, InPc@CNT and CNT.

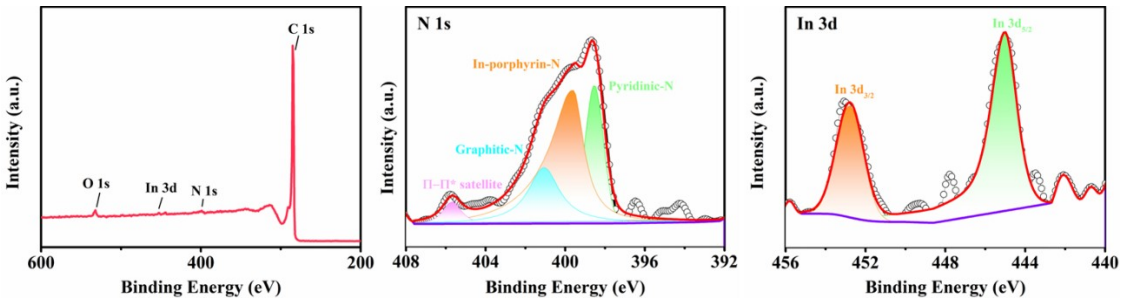

Figure S5. XPS spectra of SAIn@CNT.

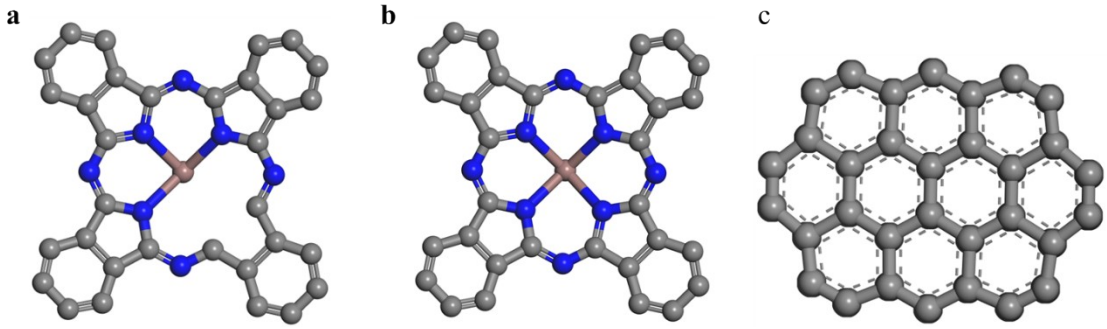

Figure S6. Structural models of a) In-N3, b) In-N4, c) CNT.

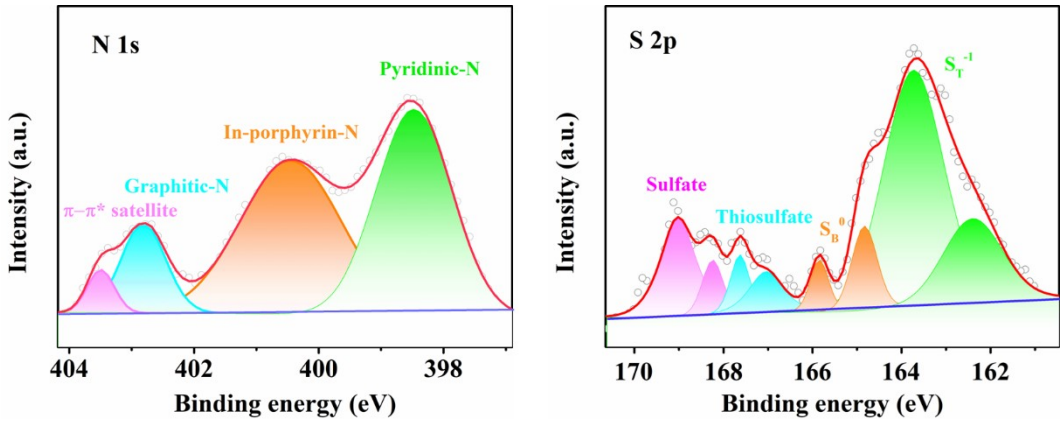

Figure S7. N 1s and S 2p XPS spectra of SAIn@CNT-Li_2S_6.

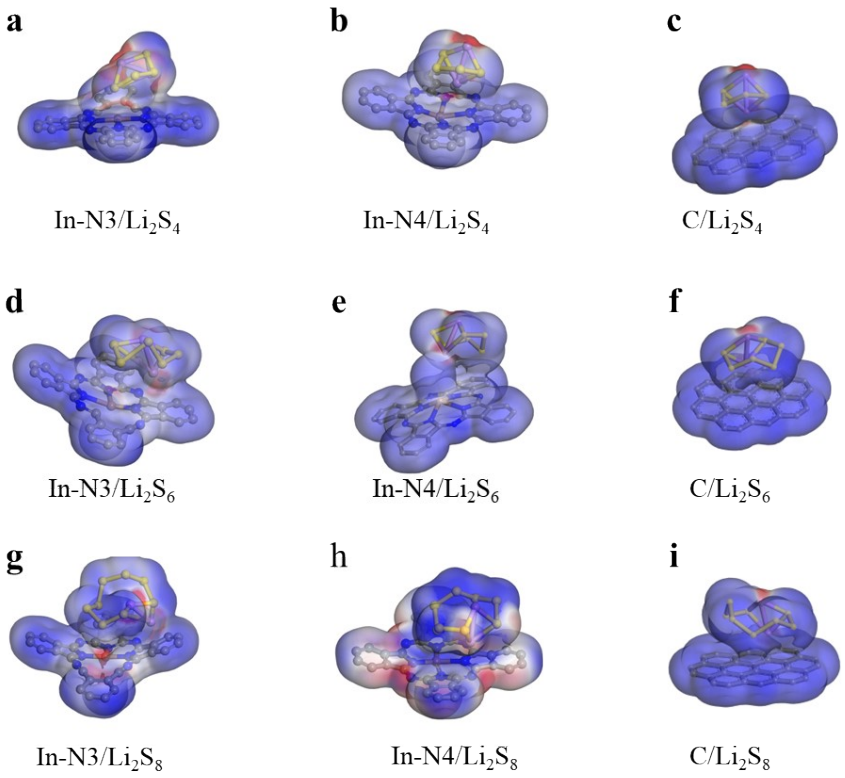

Figure S8. The optimized adsorption conformations and electrostatic potential of different sulfur species on In-N3, In-N4 and C. a, b, c) Li_2S_4, d, e, f) Li_2S_6, g, h, i) Li_2S_8. The black, gray, green and yellow represent C, N, Li and S atoms, respectively.

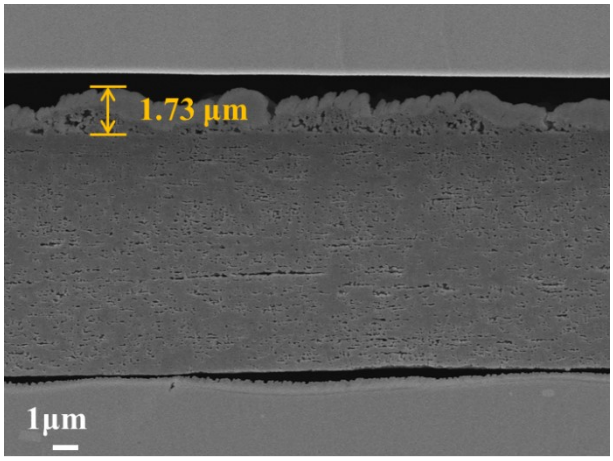

Figure S9. The cross-section of SAIn@CNT modified-separatord

Figure S10. The stability of different separators under bending and wrinkling.

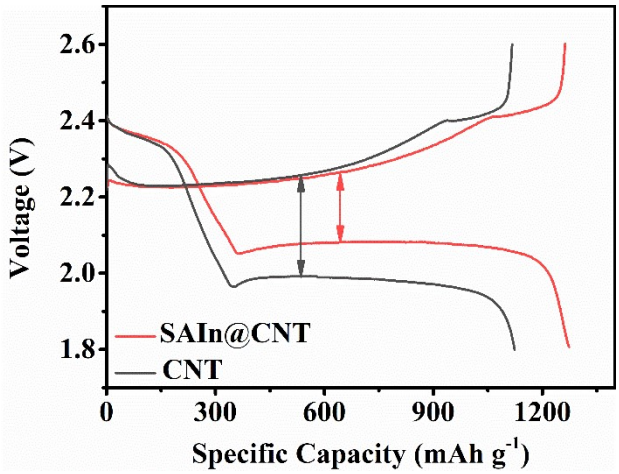

Figure S11. Galvanostatic charge/discharge profiles of coin cells with SAIn@CNT and CNT separator at 0.5 C from 1st cycle.

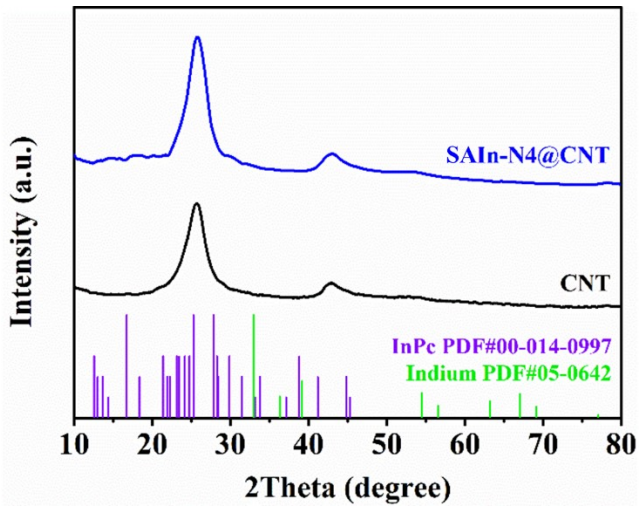

Figure S12. XRD patterns of SAIn-N4@CNT and CNT.

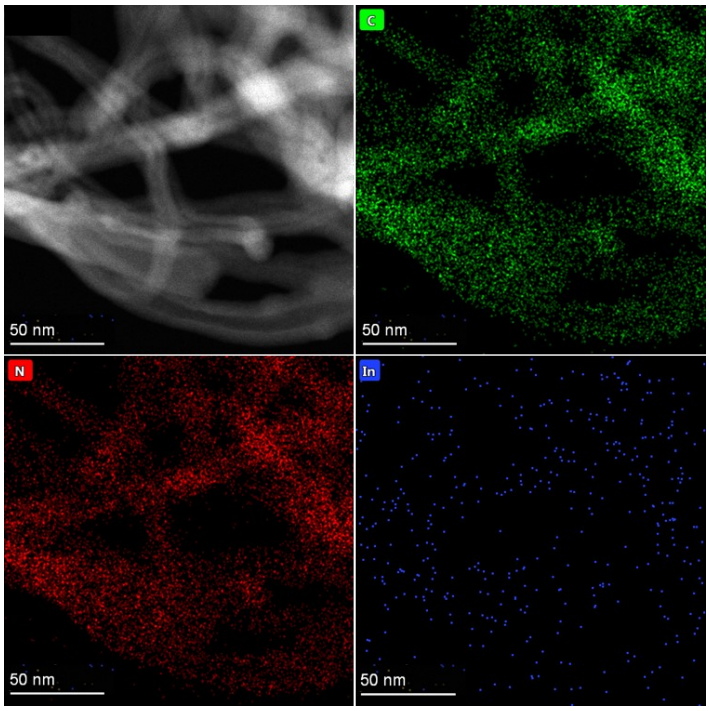

Figure S13. TEM images and corresponding elemental mapping images of SAIn-N4@CNT

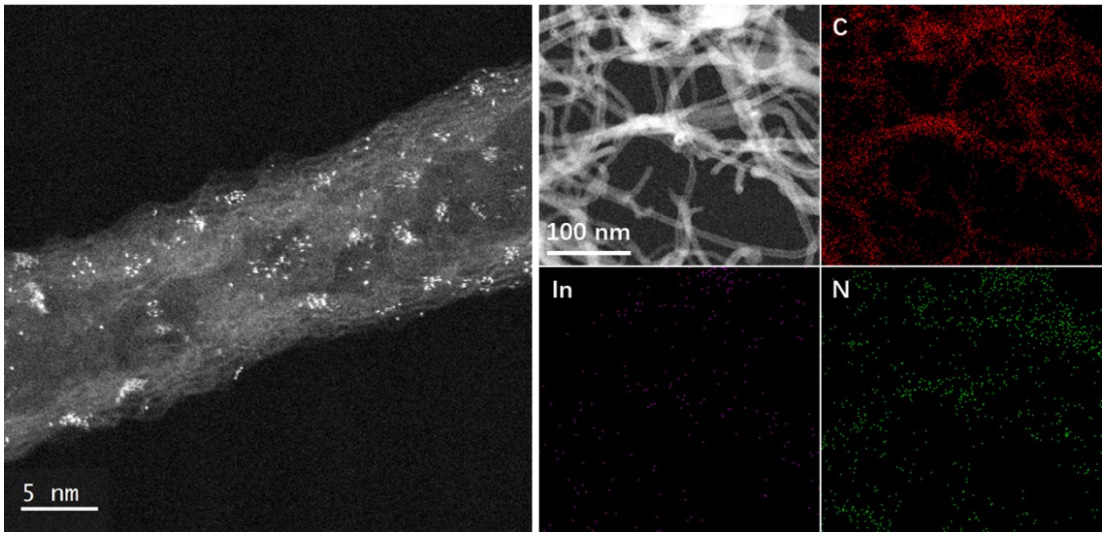

Figure S14. Characterization of structure and morphology. a) atomic-resolution HAADF-STEM image, b) STEM image and corresponding elemental mapping images of SAIn-N4@CNT

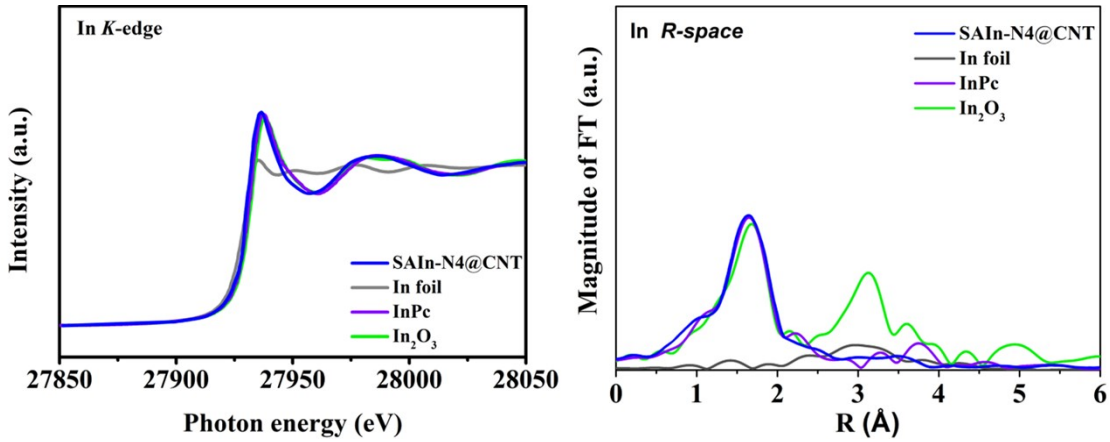

Figure S15. XANES and FT-EXAFS spectra of the SAIn-N4@CNT.

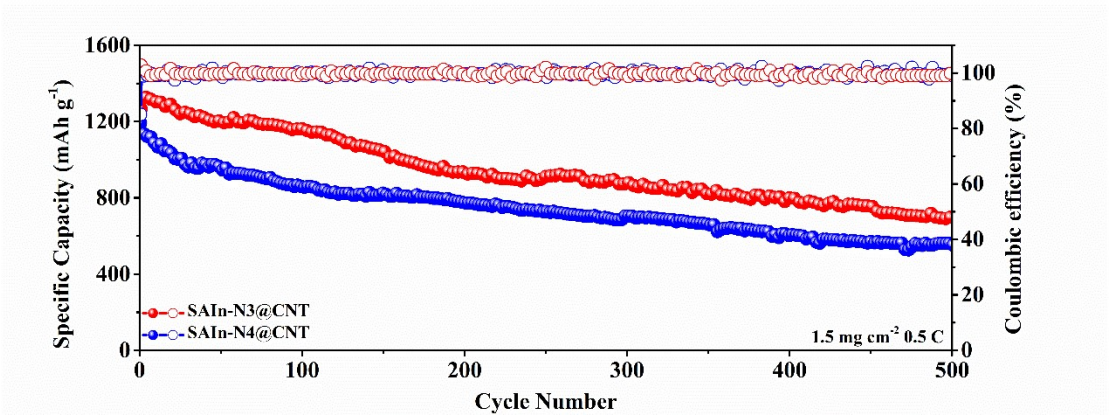

Figure S16. Cycling performance of the Li–S cells with different coordinated structure SAIn@CNT modified separators at 0.5 C.

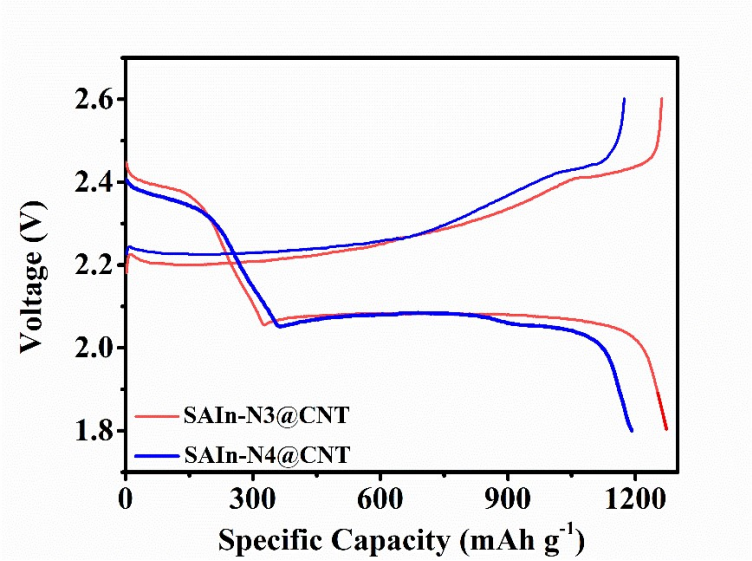

Figure S17. Galvanostatic charge/discharge profiles of coin cells with SAIn-N4@CNT and SAIn-N3@CNT separator at 0.5 C from 1st cycle.

Table S1. EXAFS fitting parameters at the In K-edge for various samples（S_0^2=0.896 for In）

Sample	Shell	*CN*[a]	*R*(Å)[b]	σ^2(Å^2)[c]	ΔE_0(eV)[d]	*R* factor
In foil	In-In	12	2.49±0.01	0.002±0.02	-8.7±1.3	0.02
In_2O_3	In-O	7.1±0.7	2.16±0.01	0.006±0.0001	2.7±1.2	0.018
	In-O-In	6.6±1.3	3.35±0.01	0.005±0.0001	1.5±1.3	
SAIn-N3@CNT	In-N	3.0±0.5	2.11±0.01	0.01±0.002	-3.7±1.8	0.02
InPc	In-N	3.8±0.4	2.11±0.01	0.005±0.001	1.5±1.3	0.01
SAIn-N4@CNT	In-N	4.0±0.6	2.11±0.01	0.005±0.002	-5.7±1.4	0.004

[a]*CN*, coordination number; [b]*R*, distance between absorber and backscatter atoms; [c]σ^2, Debye-Waller factor to account for both thermal and structural disorders; [d]ΔE_0, inner potential correction; *R* factor indicates the goodness of the fit. $S0^2$ was fixed to 0.896 for In, according to the experimental EXAFS fit of In foil by fixing CN as the known crystallographic value.

Reference

[1] WANG J, LI G, LUO D, et al. Amorphous–crystalline-heterostructured niobium oxide as two-in-one host matrix for high-performance lithium–sulfur batteries [J]. Journal of Materials Chemistry A, 2021, 9(18): 11160-7.